remote sensing

MDPI

Article

Particle Swarm Optimization-Based Noise Filtering Algorithm for Photon Cloud Data in Forest Area

Jiapeng Huang [1], Yanqiu Xing [1,*], Haotian You [2], Lei Qin [1], Jing Tian [3] and Jianming Ma [1]

[1] Centre for Forest Operations and Environment, College of Engineening and Technology, Northeast Forestry University, Harbin 150040, China; huangjp@nefu.edu.cn (J.H.); qinlei@nefu.edu.cn (L.Q.); majianming@nefu.edu.cn (J.M.)

[2] College of Geomatics and Geoinformation, Guilin University of Technology, Guilin 541004, China; yht200702@nefu.edu.cn

[3] Heilongjiang Institute of Technology, Harbin 150050, China; jing.tian@unt.edu

* Correspondence: yanqiuxing@nefu.edu.cn; Tel.: +86-451-8219-1392

Received: 14 March 2019; Accepted: 22 April 2019; Published: 24 April 2019

Abstract: The Ice, Cloud, and land Elevation Satellite-2 (ICESat-2), which is equipped with the Advanced Topographic Laser Altimeter System (ATLAS), was launched successfully in 15 September 2018. The ATLAS represents a micro-pulse photon-counting laser system, which is expected to provide more comprehensive and scientific data for carbon storage. However, the ATLAS system is sensitive to the background noise, which poses a tremendous challenge to the photon cloud noise filtering. Moreover, the Density Based Spatial Clustering of Applications with Noise (DBSCAN) is a commonly used algorithm for noise removal from the photon cloud but there has not been an in-depth study on its parameter selection yet. This paper presents an automatic photon cloud filtering algorithm based on the Particle Swarm Optimization (PSO) algorithm, which can be used to optimize the two key parameters of the DBSCAN algorithm instead of using the manual parameter adjustment. The Particle Swarm Optimization Density Based Spatial Clustering of Applications with Noise (PSODBSCAN) algorithm was tested at different laser intensities and laser pointing types using the MATLAS dataset of the forests located in Virginia, East Coast, and the West Coast, USA. The results showed that the PSODBSCAN algorithm and the localized statistical algorithm were effective in identifying the background noise and preserving the signal photons in the raw MATLAS data. Namely, the PSODBSCAN achieved the mean F value of 0.9759, and the localized statistical algorithm achieved the mean F value of 0.6978. For both laser pointing types and laser intensities, the proposed algorithm achieved better results than the localized statistical algorithm. Therefore, the PSODBSCAN algorithm could support the MATLAS photon cloud data noise filtering applicably without manually selecting parameters.

Keywords: ATLAS; MATLAS; PSO; DBSCAN; photon cloud noise filtering; forest region

1. Introduction

The Ice, Cloud, and land Elevation Satellite-2 (ICESat-2) that was successfully launched on 15 September 2018, is equipped with the Advanced Topographic Laser Altimeter System (ATLAS), and the main payload of the system is the micro-pulse photon-counting system [1]. Therefore, the system is expected to provide a reliable estimation of carbon storage [2]. Unlike the Geoscience Laser Altimeter System (GLAS) on the Ice, Cloud, and land Elevation Satellite-1 (ICESat-1), the ATLAS laser emission mode has six beams grouped in three beam pairs, each of which is composed of two different beam energies to increase system dynamic range. Each beam pair is composed of a strong beam and a weak beam, where the energy ratio of a strong beam to a weak beam is 4:1, and the right-pointed beam and

left-pointed beam of each pair denote a strong beam and a weak beam, respectively [1]. The laser emission frequency of the ATLAS laser is 10 kHz. By combining the satellite orbit and laser emission angle of the ICESat-2, it can be estimated that the diameter of the ATLAS spot on the surface is about 17 m at a 0.7 m center-to-center spacing along the track [2,3]. The center-to-center spacing along the ATLAS track is narrower than that along the GLAS track. This characteristic enables the ATLAS to obtain continuous tracking information needed for measuring the carbon storage [1,4,5]. Along with the advantages of high repetition frequency and high sensitivity, a large number of noise photons can also be received by the ATLAS system from solar and the system [4]. These noise photons can be removed by hardware devices such as range gates; however, due to fixed width characteristics of a range gate, the noise photons cannot be eliminated in the range gate [6]. Therefore, effective noise filtering is essential to retrieve signal photons from noise photons.

With the aim to improve the ICESat-2 noise filtering algorithm, different noise filtering algorithms have been tested on the airborne Sigma Space's Single Photon Lidar (SPL), Multiple Altimeter Beam Experimental Lidar (MABEL), Slope Imaging Multi-polarization Photon-counting Lidar (SIMPL), and MATLAS data released before the ICESat-2 launching [7–10]. For instance, Wang et al. [4] proposed a noise filtering based on the Bayesian method for the MABEL data. Their results showed that the algorithm could effectively distinguish signal photons from noise photons. However, the distribution of noise photons was random and related to the observation target, thus it was difficult to judge the return photon properties accurately based only on the detection probability.

Magruder et al. [11] proposed three methods, namely the modified Canny Edge Detection (CED), the Probability Distribution Function (PDF)-based signal extraction, and the localized statistical analysis for noise filtering of the photon-counting data. Their results demonstrated that the modified CED algorithm could remove noise from data of the forest area. However, the rasterized data of a signal photon could be lost, which reduced the validity of photon-counting data.

Xia et al. [12] and Xu [13] proposed a localized statistics algorithm with a center-pointed laser by using the MABEL data as experimental data. The results showed that the algorithm could effectively eliminate the noise photons. Tang et al. [14] used the SPL data as experimental data and proposed a new voxel-based spatial filtering method, which could effectively filter noise photons and retain the fine-scale canopy structure details. Nie et al. [15] proposed an effective noise removal algorithm to filter out noise photons. By using the MATLAS data as experimental data under the conditions of a laser center pointing and a strong beam, they proved that their algorithm could effectively remove noise photons from the photon cloud. However, this algorithm needed to change the threshold parameters of localized statistics artificially according to different photon densities, which significantly reduced its applicability.

Further, the Density Dimension Algorithm (DDA) and Density Based Spatial Clustering of Applications with Noise (DBSCAN) were used as noise filtering algorithms, and they were based on different densities of noise and signal photons [16–20]. Herzfeld et al. [16,17] proposed a DDA that utilized the Radial Basis Function (RBF) to calculate the weighted density as a form of data aggregation in the photon cloud and considered density as an additional parameter used as an aid in the auto-adaptive threshold determination. The experimental data included SIPML and SPL data. The experimental results showed that the algorithm had an adaptive ability and could effectively filter the noise. Popescu et al. [18] employed a multi-level noise filtering approach to classify the photons into ground and top of a canopy by using the overlapping moving window based method. The results showed that the algorithm could recognize the background noise and preserve the signal photons of the original data. Zhang et al. [19] proposed an improved DBSCAN model, whose search area was a modified horizontal ellipse, and the result showed that smoother surfaces resulted in an improved-accuracy ground height estimation. Chen et al. [20] proposed different elliptical shapes to calculate the distance between the photons and used the MATLAS data at center pointing and a strong beam to evaluate the performance of their algorithm. The results proved that the horizontal-ellipse searching area performed better than the circle and vertical-ellipse searching areas.

The DBSCAN algorithm was used to extract the signal photon in the noise filtering experiment. The algorithm used two parameters, *eps* and *MinPts*, to compare the density of data objects. For each data object in each cluster, the number of objects in an *eps*-neighborhood with a given radius had to be higher than a threshold *MinPts* [21]. The DBSCAN algorithm could efficiently cluster signal photons without target clusters and was able to discover clusters of an arbitrary shape. In the previous studies on the DBSCAN algorithm improvement, the parallel processing [22], gridding cells [23], hierarchical processing [24], combination with some other clustering algorithms [25], reduction of searching range [26], and constraints increasing [27] were used to improve the clustering accuracy and efficiency of the DBSCAN algorithm. However, the selection of the two chosen parameters (*eps* and *MinPts*) were not studied profoundly, and these parameters were set mainly by manual selection or based on an empirical formula, but these two methods could have difficulty obtaining the optimal noise filtering parameters for different experimental data. Therefore, the selection of optimal noise filtering parameters for different experimental data is still challenging and represents a research hot spot.

As a representative optimization algorithm in swarm intelligence, the Particle Swarm Optimization (PSO) algorithm has the characteristics of parallel processing and good robustness in selecting optimal parameters [28–32]. Besides, it can find the global optimal solution to a problem with a high probability, and its computational efficiency is higher than of the traditional stochastic algorithms. Consequently, it has been used in remote sensing image classification parameter optimization [28], wind forecasting model optimization [29], and medical model optimization [30,31].

Although the existing noise filtering algorithms can achieve high accuracy on the smooth surface, there are still several challenges. Namely, the noise photons are distributed over a canopy, inside a canopy, and below the ground in a forest region, which seriously affects the accuracy of signal photons extraction, which further influences the accuracy of the noise removal algorithm. At the same time, in the previous research, only strong beam type was considered without considering the laser pointing and intensity, lacking the comprehensive analysis and evaluation of the noise filtering effect. Therefore, a new algorithm for noise photon filtering at different laser pointing types and laser intensities is required.

Aiming to filter out the noise photons, a new photon cloud noise filtering algorithm named the Particle Swarm Optimization Density Based Spatial Clustering of Applications with Noise (PSODBSCAN) is proposed in this paper. The proposed algorithm integrates the global optimization search characteristics of the PSO algorithm and the density search characteristics of the DBSCAN algorithm. Namely, the PSODBSCAN algorithm uses the PSO algorithm to optimize two important parameters of the DBSCAN and then employs the optimized parameters to complete the noise filtering process such that the noise filtering result clearly describes the target height. In this paper, the MATLAS data at different laser pointing types and laser intensities on the same route over the forest region is used as test data to validate the noise filtering performance of the proposed PSODBSCAN algorithm.

The rest of the paper is organized as follows. In Section 2, the materials and methods are introduced. In Section 3, the obtained experimental results are provided. In Section 4, the discussion on the obtained experimental results is presented. Lastly, in Section 5 the main conclusions and guidelines for our future work are given.

2. Materials and Methods

2.1. Studied Area

According to the available description of MATLAS data [5], the vegetation area within the MATLAS coverage area includes Virginia, the East Coast, and the West Coast. Consequently, in this work, the studied area includes three different locations, namely Virginia, the East Coast, and the West Coast, as shown in Figure 1. There are two studied locations in Virginia, USA (77°10′19.99″W, 37°10′54.16″N), one on the East Coast, USA (78°11′33.78″W, 36°54′39.73″N), and one on the West Coast, USA (123°38′45.11″W, 44°25′56.05″N), as given in Table 1. In Table 1, Virginia 1 and Virginia 2

denote different simulation scenarios under the same observation conditions. All the studied locations are under the condition of least cloudiness. The characteristics of all the studied locations are given in Table 1.

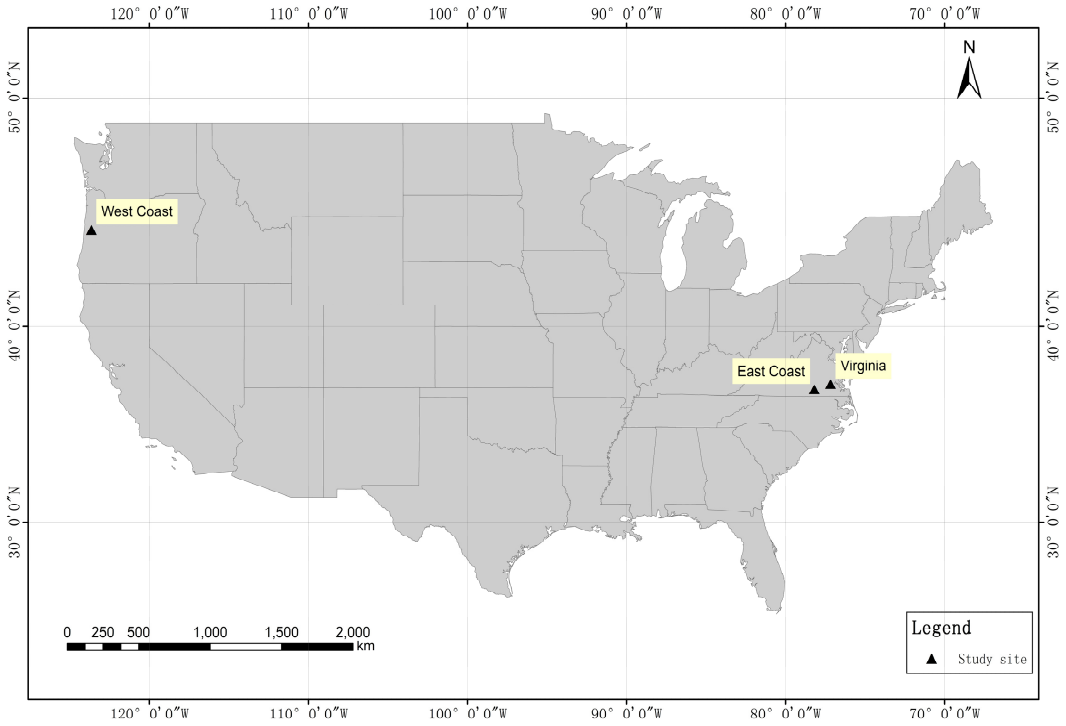

Figure 1. The studied locations.

Table 1. The characteristics of the studied locations.

Studied Site.	Studied Area	Observation Date	Observation Time	Ground Type	Canopy Closure Fraction
1	Virginia 1	20120921	22:25:00	Forest	0.55
2	Virginia 2	20120921	22:25:00	Forest	0.55
3	East Coast	20120920	23:16:00	Forest	0.90
4	West Coast	20120927	02:52:00	Forest	0.90

The studied locations are displayed in Figure 1.

2.2. Data

The MABEL was instrumented on the National Aeronautics and Space Administration (NASA) Earth Resources-2 (ER-2) high-altitude airborne scientific aircraft. The ER-2's flight altitude was 20 km above sea level (ASL). The MABEL data was acquired using a photon-counting Lidar with the pulse width of about 2 ns, the laser wavelength of 532 nm and 1064 nm, the laser energy of 5-7 μJ, the spot diameter of about 2 m, and variable pulse repetition frequency of 5-25 kHz [5,7,8,15]. In order to evaluate the performance of the ATLAS photon cloud data, NASA adjusted the photon data density, trajectory, and spatial resolution of the MABEL according to the parameters of the ATLAS instrument model to generate the MATLAS data.

The ATLAS laser beams within a pair of beams had different transmit energies, which improved the measurement accuracy within the dynamic detector range for given variations in surface reflectance [2]. The MATLAS simulated data included different laser intensities and laser pointing types and was based on the MABEL data. The MATLAS data of the center-pointing channel included an 000 channel, 043 channel, and 044 channel, and of the left-pointing channel included the 000 channel and 050 channel. Each channel included a strong beam and a weak beam.

2.3. Methodology

In this work, the PSODBSCAN algorithm based on the DBSCAN was proposed to filter out the noise photons. The new noise filtering algorithm consisted of two algorithms, the PSO algorithm and the DBSCAN algorithm, as presented in Figure 2.

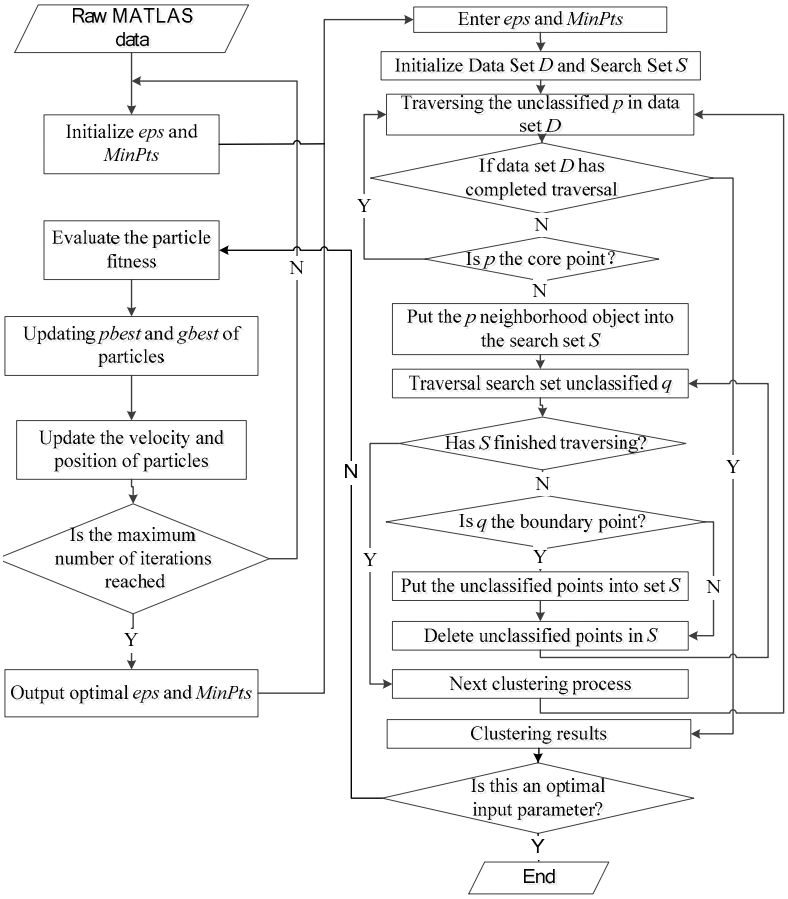

Figure 2. The flowchart of the Particle Swarm Optimization Density Based Spatial Clustering of Applications with Noise (PSODBSCAN) algorithm.

The PSO was invented by Eberhart in 1995 by simplifying the social simulation model, which was originally developed to simulate the foraging process of birds [33]. In PSO, each individual is named as a "particle" that represents a potential solution to a problem. Each particle adjusts its flying according to its own flying experience and its companions' flying experiences. Each particle is manipulated as a point in a d-dimensional space. The ith particle is represented as $X_I = (x_{i1}, x_{i2}, \ldots, x_{id})$. The best previous position (the position providing the best fitness value) of any particle is recorded and represented as $P_I = (p_{i1}, p_{i2}, \ldots, p_{id})$. The rate of the position change (velocity) of particle i is represented as $V_I(v_{i1}, v_{i2}, \ldots, v_{id})$. The particles are manipulated according to the following equations:

$$v_{id}(t+1) = w \times v_{id}(t) + c_1 \times r_1 \times (p_{id}(t) - x_{id}(t)) + c_2 \times r_2 \times (p_{gd}(t) - x_{id}(t)), \quad (1)$$

$$x_{id}(t+1) = x_{id}(t) + v_{id}(t+1), \quad (2)$$

where c_1 and c_2 are the learning factors, r_1 and r_2 are two random functions in the range [0,1], and they are different for all the dimensions and all the particles; w is the inertia weight factor, $x_{id}(t)$ is the dth position of the ith particle at time t; $p_{id}(t)$ represents the best previous position (the position providing the best fitness value) of the ith particle at the time t; further, g is the index of the best particle among all the particles in its neighborhood, $v_{id}(t)$ is the rate of the dth position change (velocity) of

particle i at time t [34]. Equations (1) and (2) define the flying velocity and trajectory of the a DBSCAN particle, respectively. Equation (1) reflects the learning and collaboration capabilities of a DBSCAN particle. The first part of Equation (1) represents the current particle velocity, the second part reflects the particle's self-learning capability, and the third part reflects the particle's collaboration capability [35]. In order to prevent the DBSCAN particles from going far away from the searching space, the particle velocity $v_{id}(t)$ is limited; otherwise, when the particle is too large, the algorithm can fly away from the optimal solution, and when it is too small, the algorithm can fall into the local optimal solution.

The DBSCAN algorithm is a density-based clustering algorithm, where the density associated with a photon is obtained by counting the photons in a region of a specified radius around that photon [36,37]. The DBSCAN has two input parameters: *eps* (the radius of *eps*-neighborhood of a photon p) and the minimum number of points (*MinPts*); *MinPts* in an *eps*-neighborhood of a photon p needs to make p a core photon of a cluster [38].

The PSODBSCAN algorithm initializes the two parameters (particles), *eps* and *MinPts*, of the DBSCAN algorithm by the PSO algorithm as input values of the DBSCAN clustering part. The PSODBSCAN algorithm starts by initializing a random photon out of the photon dataset. If a photon is not close enough to the *eps*-neighbor, the photon will be labeled as a noise photon, and the process continues to select a new photon. If a photon is sufficiently close to the *eps*-neighbor, the photon is added to the signal photon cluster. The photons are checked until the signal photon clusters are completely expanded or there are no photons left to check. A photon is defined as a "noise photon" if it does not belong to any classified signal cluster [21,39,40]. The clustering result and fitness value are calculated using the values of *eps* and *MinPts*, and then optimized by an iterative process. The optimal solution is used as an optimal parameter in the experiment, and the clustering result for the optimal parameter represents the PSODBSCAN algorithm output. The selection parameters of the PSODBSCAN algorithm are: $c_1 = 1.5$, $c_2 = 1.7$, $w = 1$, maximum speed $v_{j\max} = 100$, minimum speed $v_{j\min} = 0$, maximum number of iterations $iteration_{\max} = 100$. According to the PSO characteristics, the fraction of true signal photons that are correctly classified from all the detected signal photons is selected as an evaluation criterion of fitness.

2.4. Accuracy Evaluation

ATLAS technology is still in the airborne simulation stage, lacking evaluation criteria for noise filtering. In previous research [12,15,20], visual inspection was used as a first-step evaluation standard for photon cloud filtering. In this work, the PSODBSCAN algorithm is applied to the MATLAS data at different laser beam intensities and pointing types, and both qualitative and quantitative analyses are conducted by visual inspection using the corresponding KML file. In addition, the performances of the PSODBSCAN noise filtering algorithm including recall R, precision P, and comprehensive evaluation value F are quantitatively evaluated. Namely, R denotes the ratio of signal photons that are successfully detected to all the true signal photons, P denotes the ratio of true signal photons that are correctly classified to all the detected signal photons, and F denotes the harmonic mean of recall and precision. These three indicators are calculated using the reference classification data [15,20], and they are respectively given by:

$$R = TP/(TP + FN), \tag{3}$$

$$P = TP/(TP + FP), \tag{4}$$

$$F = 2 \times P \times R/(P + R), \tag{5}$$

where TP, FP, and FN denote the numbers of true positives, false positives, and false negatives, respectively. To be more specific, true positives represent the true signal photons that are correctly detected, false positives are the noise photons that are misclassified as signal photons, and false negatives stand for the true signal photons that are not correctly detected. To test the applicability of the PSODBSCAN algorithm, the PSODBSCAN algorithm was compared with the localized statistics algorithm proposed by Xia et al. [12].

3. Results

3.1. Noise Filtering Under Strong Beams

3.1.1. Noise Filtering Under Laser Center Pointing

The noise filtering results of the PSODBSCAN algorithm and the localized statistics algorithm over the Virginia 1 flight line channel 043 under the strong beam and center pointing are presented in Figure 3. The statistical indicators, namely the *R*, *P*, and *F* values, of the PSODBSCAN algorithm and the localized statistics algorithm over the Virginia 1, Virginia 2, East Coast, and West Coast flight line channels 000, 043, and 044 under the strong beam are given in Tables 2–4, respectively.

Table 2. The *R* value of the noise filtering algorithms under the strong beam and center pointing.

Algorithm	**Localized Statistics**			**PSODBSCAN**		
Channel	**000**	**043**	**044**	**000**	**043**	**044**
Virginia 1	1.0000	1.0000	1.0000	0.9993	1.0000	1.0000
Virginia 2	1.0000	1.0000	1.0000	1.0000	0.9998	1.0000
East Coast	1.0000	1.0000	1.0000	0.9997	1.0000	1.0000
West Coast	1.0000	1.0000	1.0000	0.9997	1.0000	1.0000
Mean of channel	1.0000	1.0000	1.0000	0.9997	0.9999	1.0000
Mean of algorithmic result		1.0000			0.9999	

Table 3. The *P* value of the noise filtering algorithms under the strong beam and center pointing.

Algorithm	**Localized Statistics**			**PSODBSCAN**		
Channel	**000**	**043**	**044**	**000**	**043**	**044**
Virginia 1	0.9239	0.9457	0.9512	0.9658	0.9907	0.9962
Virginia 2	0.9900	0.9778	0.9200	0.9993	0.9965	0.9652
East Coast	0.9844	0.9852	0.9453	0.9922	0.9940	0.9549
West Coast	0.9913	0.9940	0.9944	0.9962	0.9991	0.9991
Mean of channel	0.9724	0.9757	0.9527	0.9884	0.9951	0.9788
Mean of algorithmic result		0.9669			0.9874	

Table 4. The *F* value of the noise filtering algorithms under the strong beam and center pointing.

Algorithm	**Localized statistics**			**PSODBSCAN**		
Channel	**000**	**043**	**044**	**000**	**043**	**044**
Virginia 1	0.9604	0.9721	0.9749	0.9822	0.9953	0.9980
Virginia 2	0.9949	0.9887	0.9583	0.9996	0.9981	0.9823
East Coast	0.9921	0.9925	0.9718	0.9959	0.9970	0.9769
West Coast	0.9956	0.9970	0.9971	0.9979	0.9995	0.9995
Mean of channel	0.9858	0.9876	0.9755	0.9939	0.9975	0.9913
Mean of algorithmic result		0.9829			0.9935	

By comparing results presented in Figure 3b,c, it can be concluded that the PSODBSCAN removed more noise photons than the localized statistics algorithm. In Figure 3e, the square areas denote the canopy photons, and the elliptical area denotes the ground photons. Comparing the results presented in Figure 3d,e, it can be noticed that the PSODBSCAN showed a clearer depiction of the ground vegetation than the localized statistics algorithm.

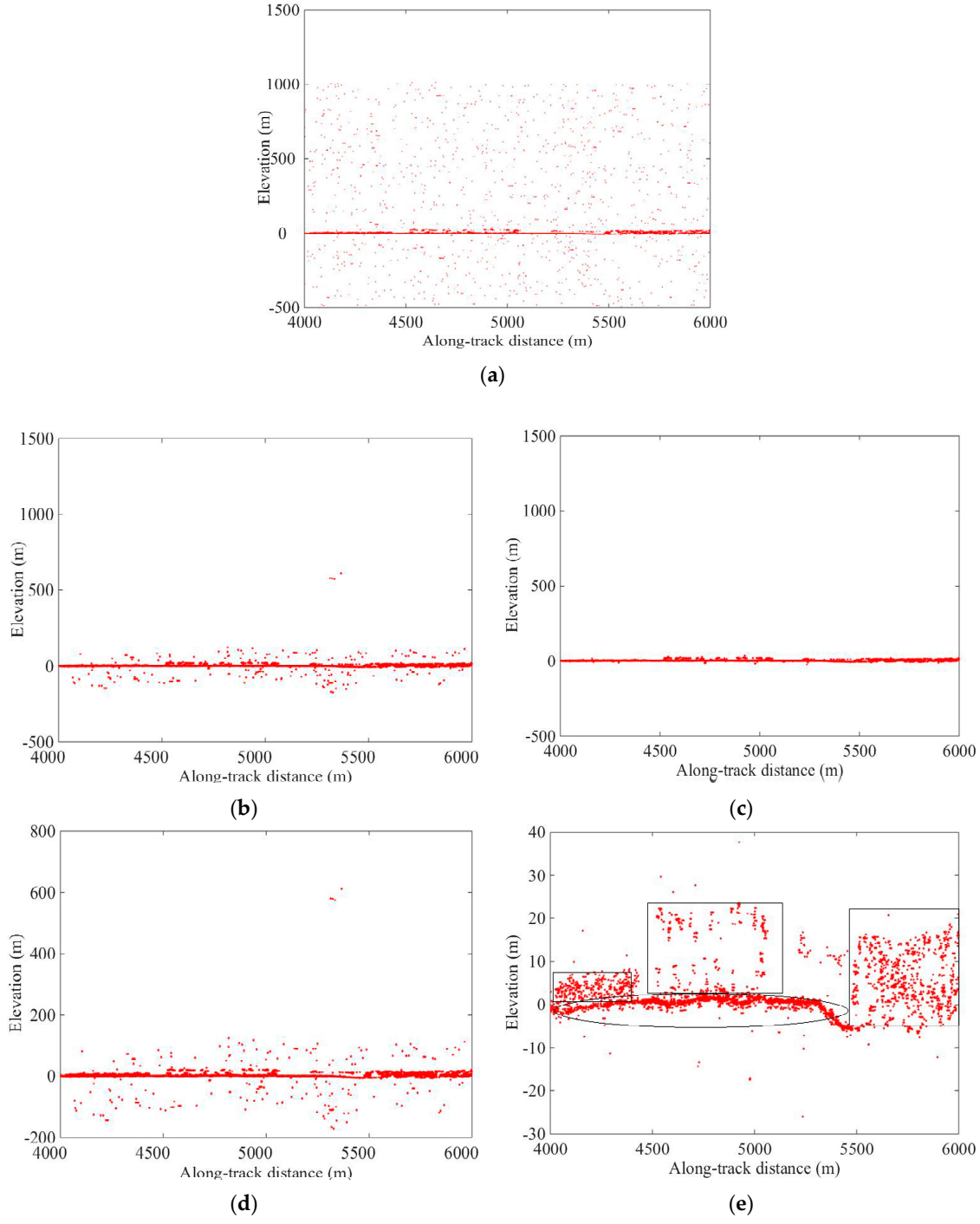

Figure 3. The noise filtering results of the PSODBSCAN algorithm and the localized statistics algorithm over the Virginia 1 flight line channel 043 under the strong beam and center pointing. (**a**) Raw data; (**b**) the noise filtering result of the localized statistics algorithm; (**c**) the noise filtering result of the PSODBSCAN algorithm; (**d**) the noise filtering result of the localized statistics algorithm (the enlarged view of a part of the result presented in figure (**b**)); (**e**) the noise filtering result of the PSODBSCAN algorithm (the enlarged view of a part of the result presented in figure (**c**)); the square areas denote the canopy photons and the elliptical area denotes the ground photons.

As given in Tables 2–4, the PSODBSCAN algorithm achieved the mean *R*, *P*, and *F* values of 0.9999, 0.9874, and 0.9935, respectively, and the localized statistics algorithm achieved the mean *R*, *P*, and *F*

values of 1.0000, 0.9669, and 0.9829, respectively. Thus, the PSODBSCAN algorithm achieved similar *R* value, but higher *P* and *F* values than the localized statistics algorithm.

In summary, results in Tables 2–4 and Figure 3 show that the PSODBSCAN algorithm performed much better than the localized statistics algorithm. Accordingly, the PSODBSCAN algorithm could remove the noise photons more effectively than the localized statistics algorithm under the strong beam and center pointing.

3.1.2. Noise Filtering Under Laser Left Pointing

The noise filtering results of the PSODBSCAN algorithm and the localized statistics algorithm over the Virginia 1 flight line channel 000 under the strong beam and left pointing are presented in Figure 4. The statistical indicators, namely the *R*, *P*, and *F* values, of the PSODBSCAN algorithm and the localized statistics algorithm over the Virginia 1, Virginia 2, East Coast, and West Coast flight line channels 000 and 050 under the strong beam are given in Tables 5–7, respectively.

Table 5. The *R* value of the noise filtering algorithms under the strong beam and left pointing.

Algorithm	**Localized Statistics**		**PSODBSCAN**	
Channel	**000**	**050**	**000**	**050**
Virginia 1	1.0000	1.0000	0.9998	1.0000
Virginia 2	1.0000	1.0000	1.0000	1.0000
East Coast	1.0000	1.0000	1.0000	1.0000
West Coast	1.0000	1.0000	1.0000	0.9997
Mean of channel	1.0000	1.0000	0.9999	0.9999
Mean of algorithmic result	1.0000		0.9999	

Table 6. The *P* value of the noise filtering algorithms under the strong beam and left pointing.

Algorithm	**Localized Statistics**		**PSODBSCAN**	
Channel	**000**	**050**	**000**	**050**
Virginia 1	0.8802	0.8579	0.9920	0.9885
Virginia 2	0.9200	0.9153	0.9652	0.9709
East Coast	0.9881	0.9889	0.9989	0.9971
West Coast	0.9944	0.9900	0.9990	0.9967
Mean of channel	0.9457	0.9380	0.9888	0.9883
Mean of algorithmic result	0.9419		0.9885	

Table 7. The *F* value of the noise filtering algorithms under the strong beam and left pointing.

Algorithm	**Localized Statistics**		**PSODBSCAN**	
Channel	**000**	**050**	**000**	**050**
Virginia 1	0.9362	0.9235	0.9958	0.9941
Virginia 2	0.9583	0.9558	0.9823	0.9852
East Coast	0.9940	0.9944	0.9994	0.9985
West Coast	0.9971	0.9949	0.9995	0.9982
Mean of channel	0.9714	0.9672	0.9943	0.9940
Mean of algorithmic result	0.9693		0.9942	

Figure 4 shows the noise filtering results of the PSODBSCAN algorithm and the localized statistics algorithm over the Virginia 1 flight line channel 000 under the strong beam and left pointing. As presented in Figure 4b,c, the result of the PSODBSCAN contained fewer noise photons than that of the localized statistics algorithm. In Figure 4e, the square areas denote the canopy photons, and the elliptical area denotes the ground photons. Comparing the results presented in Figure 4d,e, it can

be seen that the PSODBSCAN algorithm performed better than the localized statistics algorithm in ground vegetation (i.e., the results obtained by the PSODBSCAN algorithm were clearer).

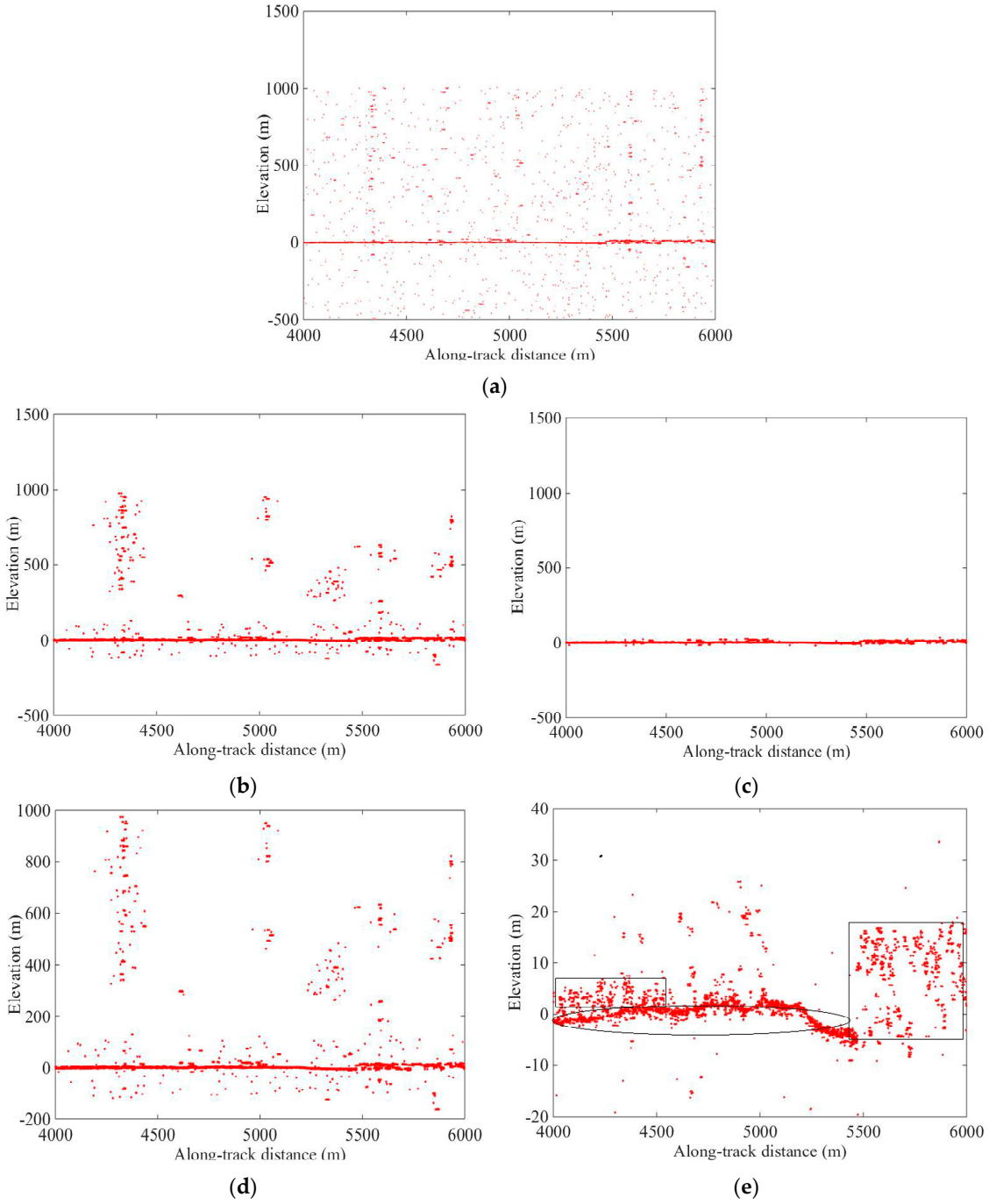

Figure 4. The noise filtering results of the PSODBSCAN algorithm and the localized statistics algorithm over the Virginia 1 flight line channel 000 under the strong beam and left pointing. (**a**) Raw data; (**b**) the noise filtering result of the localized statistics algorithm; (**c**) the noise filtering result of the PSODBSCAN algorithm; (**d**) the noise filtering result of the localized statistics algorithm (the enlarged view of a part of the result presented in figure (**b**)); (**e**) the noise filtering result of the PSODBSCAN algorithm (the enlarged view of a part of the result presented in figure (**c**)); the square areas denote the canopy photons, and the elliptical area denotes the ground photons.

The PSODBSCAN algorithm achieved the mean *R*, *P*, and *F* values of 0.9999, 0.9885, and 0.9942, respectively, and the localized statistics algorithm achieved the mean *R*, *P*, and *F* values of 1.0000, 0.9419, and 0.9693, respectively, as presented in Tables 5–7. Accordingly, the PSODBSCAN algorithm performed better than the localized statistics algorithm under the strong beam and left pointing.

Comparing the results given in Tables 2–7, which were obtained under the strong beam, it can be seen that the PSODBSCAN algorithm achieved the mean *R*, *P*, and *F* values of 0.9999, 0.9879, and 0.9938, respectively, while the localized statistics algorithm achieved the mean *R*, *P*, and *F* values of 1.0000, 0.9569, and 0.9775, respectively. The experimental results showed that under the strong beam, the PSODBSCAN algorithm could remove the noise photon more effectively than the localized statistics algorithm.

3.2. Noise Filtering Under Weak Beams

3.2.1. Noise Filtering Under Laser Center Pointing

The noise filtering results of the PSODBSCAN algorithm and the localized statistics algorithm over the East Coast flight line channel 043 under the weak beam and center pointing are presented in Figure 5. The statistical indicators, namely the *R*, *P*, and *F* values, of the PSODBSCAN algorithm and the localized statistics algorithm over the Virginia 1, Virginia 2, East Coast, and West Coast flight line channels 000, 043, and 044 under the weak beam are given in Tables 8–10, respectively.

Table 8. The *R* value of the noise filtering algorithms under the weak beam and center pointing.

Algorithm	**Localized Statistics**			**PSODBSCAN**		
Channel	**000**	**043**	**044**	**000**	**043**	**044**
Virginia 1	0.9181	0.8052	0.4855	1.0000	1.0000	1.0000
Virginia 2	0.7111	0.4762	1.0000	1.0000	1.0000	0.9981
East Coast	0.0000	0.1419	0.0787	1.0000	0.9989	1.0000
West Coast	0.0000	0.0180	0.0000	1.0000	1.0000	1.0000
Mean of channel	0.4073	0.3603	0.3910	1.0000	0.9997	0.9995
Mean of algorithmic result		0.3862			0.9997	

Table 9. The *P* value of the noise filtering algorithms under the weak beam and center pointing.

Algorithm	**Localized Statistics**			**PSODBSCAN**		
Channel	**000**	**043**	**044**	**000**	**043**	**044**
Virginia 1	0.9933	0.9747	0.7813	0.9878	0.9509	0.7811
Virginia 2	0.9223	0.9850	0.9200	0.9225	0.9489	0.9832
East Coast	0.0000	1.0000	0.9722	0.9242	0.9911	0.9834
West Coast	0.0000	1.0000	0.0000	0.9949	0.9905	0.9889
Mean of channel	0.4789	0.9899	0.6684	0.9574	0.9703	0.9342
Mean of algorithmic result		0.7124			0.9540	

Table 10. The *F* value of the noise filtering algorithms under the weak beam and center pointing.

Algorithm	**Localized Statistics**			**PSODBSCAN**		
Channel	**000**	**043**	**044**	**000**	**043**	**044**
Virginia 1	0.9542	0.8818	0.5988	0.9938	0.9748	0.8771
Virginia 2	0.8030	0.6421	0.9583	0.9596	0.9737	0.9906
East Coast	0.0000	0.2485	0.1455	0.9607	0.9949	0.9916
West Coast	0.0000	0.0353	0.0000	0.9974	0.9952	0.9944
Mean of channel	0.4393	0.4519	0.4256	0.9778	0.9846	0.9634
Mean of algorithmic result		0.4389			0.9753	

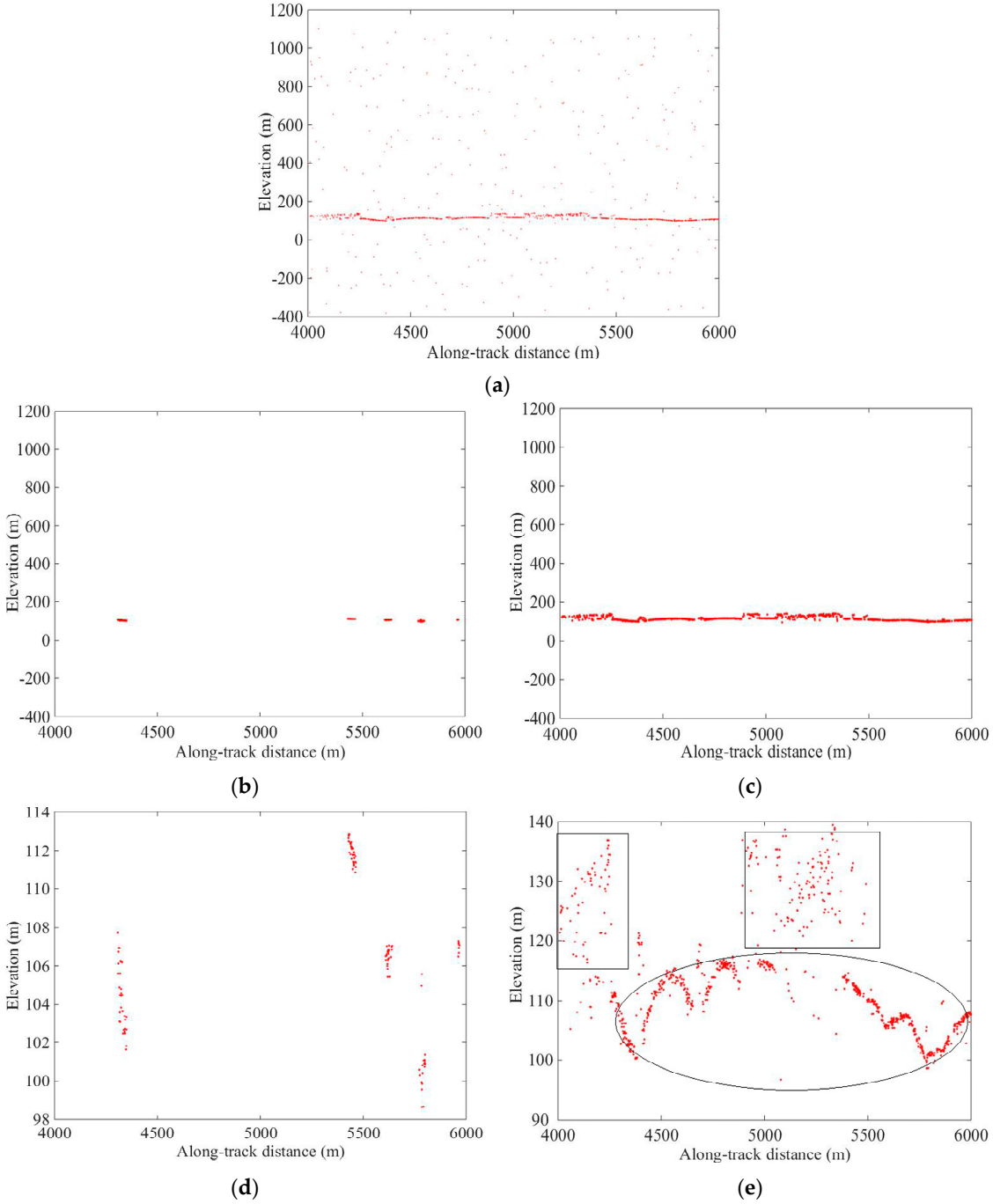

Figure 5. The noise filtering results of the PSODBSCAN algorithm and the localized statistics algorithm over the East Coast flight line channel 043 under the weak beam and center pointing. (**a**) Raw data; (**b**) the noise filtering result of the localized statistics algorithm; (**c**) the noise filtering result of the PSODBSCAN algorithm; (**d**) the noise filtering result of the localized statistics algorithm(the enlarged view of a part of the result presented in figure (**b**)); (**e**) the noise filtering result of the PSODBSCAN algorithm(the enlarged view of a part of the result presented in figure (**c**)); the square areas denote the canopy photons, and the elliptical area denotes the ground photons.

As presented in Figure 5b, the localized statistics algorithm filtered the noise and signal photons in the forest region. However, the PSODBSCAN algorithm not only acquired more signal photons but also filtered the noise photons better than the localized statistics algorithm. In Figure 5e, the square areas denote the canopy photons, and the elliptical area denotes the ground photons. Comparing the

results presented in Figure 5d,e, it can be concluded that the PSODBSCAN algorithm performed better than the localized statistics algorithm in ground vegetation.

Besides, the PSODBSCAN algorithm achieved the mean *R*, *P*, and *F* values of 0.9997, 0.9540, and 0.9753, respectively, and the localized statistics algorithm achieved the mean *R*, *P*, and *F* values of 0.3862, 0.7124, and 0.4389, respectively, as given in Tables 8–10. Tables 8–10 also show that the localized statistics algorithm achieved the *R*, *P*, and *F* values of about 0 over the East Coast and the West Coast, while the PSODBSCAN algorithm achieved higher *F* value in those areas, thus performing much better than the localized statistics algorithm.

Comparing the results given in Tables 2–4 and Tables 8–10, it can be noticed that the PSODBSCAN algorithm achieved the mean *R*, *P*, and *F* values of 0.9998, 0.9707, and 0.9844, respectively, while the localized statistics algorithm achieved the mean *R*, *P*, and *F* values of 0.6931, 0.8397, and 0.7110, respectively. Thus, the PSODBSCAN algorithm removed the noise photon more effectively than the localized statistics algorithm under the center pointing.

3.2.2. Noise Filtering Under Laser Left Pointing

The noise filtering results of the PSODBSCAN algorithm and the localized statistics algorithm over the East Coast flight line channel 000 under the weak beam and left pointing are presented in Figure 6. The statistical indicators, namely the *R*, *P*, and *F* values, of the PSODBSCAN algorithm and the localized statistics algorithm over the Virginia 1, Virginia 2, East Coast, and West Coast flight line channels 000 and 050 under the weak beam are given in Tables 11–13, respectively.

Table 11. The *R* value of noise filtering algorithms under the weak beam and left pointing.

Algorithm	**Localized Statistics**		**PSODBSCAN**	
Channel	**000**	**050**	**000**	**050**
Virginia 1	0.4525	0.4808	1.0000	1.0000
Virginia 2	0.9231	0.5535	1.0000	1.0000
East Coast	0.1055	0.1151	1.0000	1.0000
West Coast	0.0000	0.0000	0.9812	1.0000
Mean of channel	0.3703	0.2874	0.9953	1.0000
Mean of algorithmic result	0.3288		0.9977	

Table 12. The *P* value of noise filtering algorithms under the weak beam and left pointing.

Algorithm	**Localized Statistics**		**PSODBSCAN**	
Channel	**000**	**050**	**000**	**050**
Virginia 1	0.7523	0.7642	0.7556	0.7392
Virginia 2	0.9692	0.8048	0.9596	0.8165
East Coast	1.0000	1.0000	0.9763	0.9922
West Coast	0.0000	0.0000	0.9212	0.9414
Mean of channel	0.6804	0.6423	0.9032	0.8723
Mean of algorithmic result	0.6613		0.8877	

Table 13. The *F* value of noise filtering algorithms under the weak beam and left pointing.

Algorithm	**Localized Statistics**		**PSODBSCAN**	
Channel	**000**	**050**	**000**	**050**
Virginia 1	0.5651	0.5902	0.8608	0.8500
Virginia 2	0.9455	0.6559	0.9793	0.8990
East Coast	0.1907	0.2064	0.9880	0.9961
West Coast	0.0000	0.0000	0.9502	0.9698
Mean of channel	0.4253	0.3631	0.9445	0.9287
Mean of algorithmic result	0.3942		0.9367	

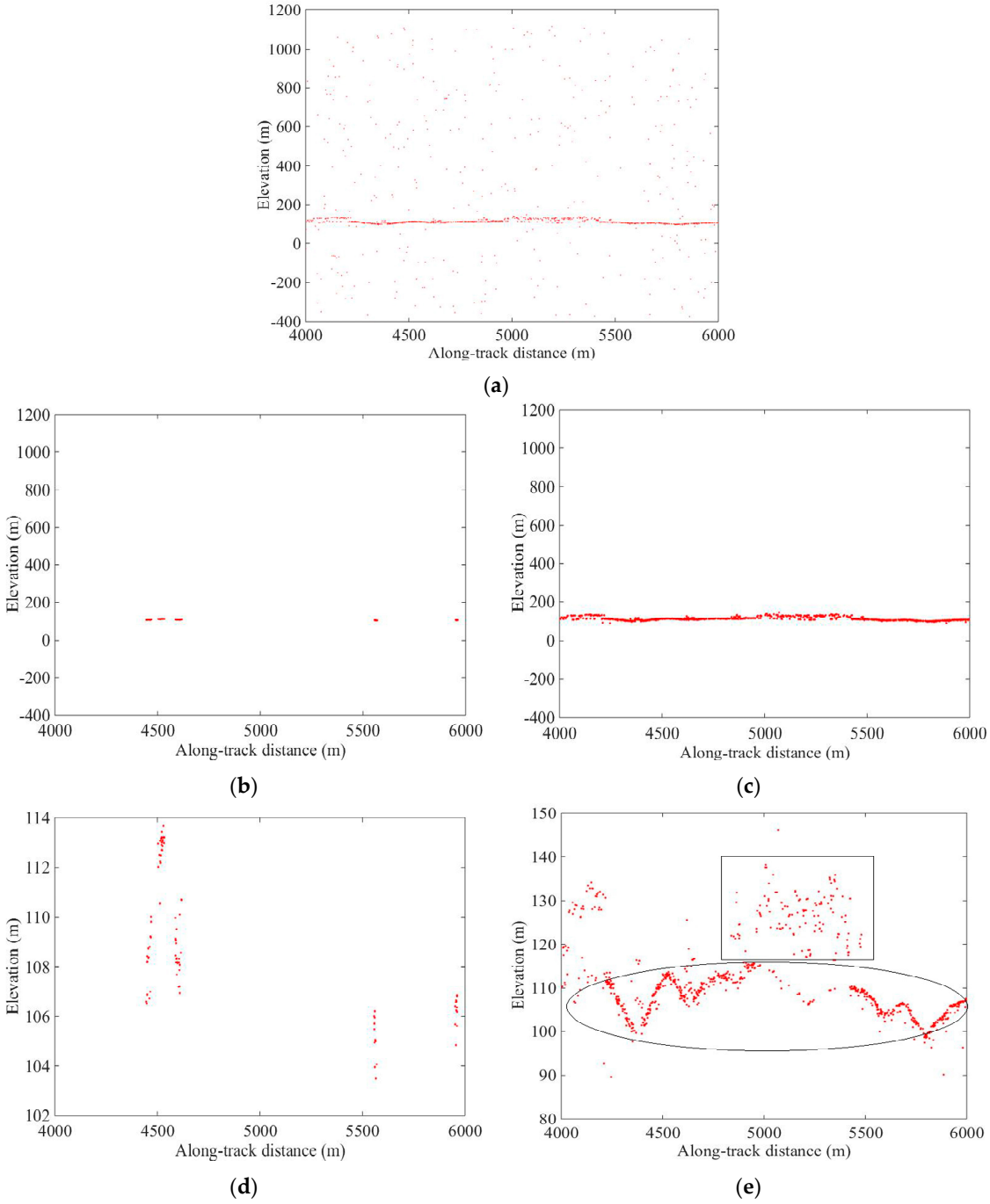

Figure 6. The noise filtering results of the PSODBSCAN algorithm and the localized statistics algorithm over the East Coast flight line channel 000 under the weak beam and left pointing. (**a**) Raw data; (**b**) the noise filtering result of the localized statistics algorithm; (**c**) the noise filtering result of the PSODBSCAN algorithm; (**d**) the noise filtering result of the localized statistics algorithm (the enlarged view of a part of the result presented in figure (**b**)); (**e**) the noise filtering result of the PSODBSCAN algorithm (the enlarged view of a part of the result presented in figure (**c**)); the square area denotes the canopy photons, and the elliptical area denotes the ground photons.

As shown in Figure 6b, the localized statistics algorithm retained only a part of the signal photons in the forest region. On the other hand, as presented in Figure 6c, the PSODBSCAN algorithm not only retained much more signal photons but also filtered the noise photons. In Figure 6e, the square area denotes the canopy photons, and the elliptical area denotes the ground photons. Comparing the

results presented in Figure 6d,e, it can be seen that the PSODBSCAN algorithm performed better than the localized statistics algorithm in both ground and forest.

As given in Tables 11–13, the PSODBSCAN algorithm achieved the mean *R*, *P*, and *F* values of 0.9977, 0.8877, and 0.9367, respectively, and the localized statistics algorithm achieved the mean *R*, *P*, and *F* values of 0.3288, 0.6613, and 0.3942, respectively. Tables 11–13 also show that the localized statistics algorithm achieved the mean *R*, *P*, and *F* values of about 0 over the West Coast, while the PSODBSCAN algorithm obtained higher *R*, *P*, and *F* values in that area, thus performing much better than the localized statistics algorithm.

As given in Tables 5–7 and Tables 11–13, the PSODBSCAN algorithm achieved the mean *R*, *P*, and *F* values of 0.9988, 0.9381, and 0.9654, respectively, and the localized statistics algorithm achieved the mean *R*, *P*, and *F* values of 0.6644, 0.8016, and 0.6818, respectively. The experimental results showed that the PSODBSCAN algorithm removed the noise photon more effectively than the localized statistics algorithm under the left pointing.

4. Discussion

There is considerable interest in developing an effective noise filtering algorithm needed to conduct an accurate canopy height measurement from the MATLAS data. The proposed PSODBSCAN algorithm addresses some of the drawbacks of the localized statistics algorithm [12], offering a suitable solution for noise filtering from the MATLAS data.

4.1. Noise Filtering Results at Different Beam Intensities

The mean statistical indicators of the PSODBSCAN algorithm and the localized statistics algorithm at different beam intensities are given in Table 14.

Table 14. The mean statistical indicators of noise filtering algorithms at different beam intensities.

Algorithm	**Localized Statistics**		**PSODBSCAN**	
Beam Intensity	**Strong**	**Weak**	**Strong**	**Weak**
R	1.0000	0.3633	0.9999	0.9989
P	0.9569	0.6920	0.9879	0.9275
F	0.9775	0.4211	0.9938	0.9599

The previous studies suggested that variation in the MATLAS data density, caused by the differences in the photon cloud at studied locations [15], is an important factor, which should be considered at different laser intensities. In our experiments, the density of signal photons was higher under the strong beam than under the weak laser beam.

The qualitative analysis results are summarized in Figures 3–6. According to the presented results, under the strong beam, the densities of forest photons and ground photons were particularly discernible, and both noise filtering algorithms could remove the noise photons. However, under the weak laser beam, the densities of forest photons and ground photons could not be clearly described, and only a part of the signal photons was retrieved by the localized statistics algorithm, while the PSODBSCAN algorithm retrieved much more signal photons in studied areas.

The quantitative analysis results are summarized in Table 14, where it is shown that under the strong beam and weak beam, the PSODBSCAN algorithm achieved the mean *F* value of 0.9938 and 0.9599, respectively, while the localized statistics algorithm achieved the mean *F* value of 0.9775 and 0.4211, respectively. The mean *F* value of the localized statistics algorithm was about 0.42 at different laser intensities, while the mean *F* value of the PSODBSCAN algorithm was consistently better than 0.95. Thus, the PSODBSCAN algorithm was more effective than the localized statistics algorithm for the MATLAS photon cloud at all laser intensities, which was due to several reasons. First, the PSODBSCAN algorithm performed better in noise photons filtering (i.e., it achieved higher *R*, *P*, and

F values) than the localized statistics algorithm because the PSODBSCAN had the characteristics of local search and clusters of arbitrary shapes with a density as a criterion. Therefore, the PSODBSCAN algorithm did not cluster signal photons according to the threshold of a local statistical distance, avoiding the loss of canopy photons and ground photons. Moreover, the localized statistics algorithm eliminated the noise photons using a fixed threshold; thus, errors appeared at a low density where the ground and canopy were difficult to the identify in the photon cloud, especially under the weak laser beam. Second, the localized statistics algorithm needed to adjust the key parameters according to different laser intensity; however, it did not adjust the test parameters manually according to different laser intensity, resulting in the *F* value of about 0.20 or even 0 under the weak beam condition. Manual parameter adjustment has been known to affect noise filtering efficiency and accuracy. Although the potential correction methods (e.g., factor adjusting procedures) may help to improve the noise filtering accuracy [15], the final performance largely depends on manual adjustment of parameters, thus these methods are not suitable to be implemented globally due to their specificity.

Notably, the visual inspection revealed that a part of the signal photons was removed by the localized statistics algorithm (see Figure 5b, and Figure 6b and Tables 10 and 13). Besides, the localized statistics algorithm achieved the mean *F* value of 0 over the East Coast and West Coast under the weak beam. By analyzing the characteristics of the local statistical algorithm, the obtained results could be explained by the two following facts. Namely, there was a lower density of signal photon in the region, and the distance statistics sum of the signal photons exceeded the threshold of the local statistical algorithm. Therefore, it was difficult to remove the noise photons in the forest and ground regions by the localized statistics algorithm. Moreover, analyzing the test results of the localized statistics algorithm, it was concluded that test parameters affected the noise filtering effect of the localized statistics algorithm. Thus, it was necessary to adjust the algorithm parameters according to a different density of test data. In this work, the parameters were not selected based on test settings but set to the values used in reference [12]. Both qualitative and quantitative results indicated that the PSODBSCAN algorithm performed better than the localized statistics algorithm, and the PSODBSCAN algorithm did not need manual parameter adjustment to different test data.

Moreover, the noise filtering results of the two algorithms under the strong beam were better than under the weak beam. The signal photon density under the strong beam conditions was higher than under the weak beam conditions, and it could be obviously noticed that ground and canopy photons under the strong beam condition (see Figures 3 and 4). Therefore, a higher density of signal photons improved the noise filtering ability of both algorithms.

Overall, the qualitative and quantitative results indicated that the PSODBSCAN algorithm performed better than the localized statistics algorithm in noise photon filtering under both strong beam and weak beam.

4.2. Noise Filtering Results at Different Laser Pointing Types

The mean statistical indicators of the PSODBSCAN algorithm and the localized statistics algorithm at different laser pointing types are given in Table 15.

Table 15. The mean statistical indicators of noise filtering algorithms at different laser pointing types.

Algorithm	**Localized Statistics**		**PSODBSCAN**	
Laser Pointing	**Center**	**Left**	**Center**	**Left**
R	0.6931	0.6644	0.9998	0.9988
P	0.8397	0.8016	0.9707	0.9381
F	0.7110	0.6818	0.9844	0.9654

The previous studies suggested that variation in the MATLAS data density, caused by the differences in the photon cloud at studied locations, is an important factor, which should be considered at different laser pointing types. In our experiments, the density of signal photons was higher under

the center pointing than under the left pointing. The qualitative analysis results are presented in Figures 3–6. Under the condition of center pointing, the densities of forest photons and ground photons were more obviously discernible than under the left pointing. The visual inspection revealed that a part of the signal photons was removed by the localized statistics algorithm under the left pointing, while the PSODBSCAN algorithm obtained more signal photons in those areas (see Figures 4 and 6).

The quantitative analysis results are summarized in Table 15. Based on these results, under the center pointing and left pointing, the PSODBSCAN algorithm achieved a mean F value of 0.9844 and 0.9654, respectively, and the localized statistics algorithm achieved a mean F value of 0.7110 and 0.6818, respectively. The mean *F* value of the localized statistics algorithm was about 0.68, while the mean *F* value of the PSODBSCAN algorithm was higher than 0.96. The comparison results indicated that the PSODBSCAN algorithm was more effective than the localized statistics algorithm for the MATLAS photon cloud at different beam pointing types, which was due to several reasons. First, the PSODBSCAN algorithm achieved consistently better accuracy in noise photon filtering (i.e., it achieved higher *R*, *P*, and *F* values) than the localized statistics algorithm. The main reason for this was that the localized statistics algorithm resulted in a loss of canopy photons and ground photons due to the fixed threshold, while the PSODBSCAN algorithm identified the noise cluster based on the signal photon density. Therefore, the localized statistics algorithm failed to remove the noise at a lower density where the ground and canopy were difficult to identify in the photon cloud (left pointing). Second, the localized statistics algorithm should have adjusted the key parameters according to different test data; however, it did not adjust all the test parameters according to different laser pointing data, resulting in the *F* value of about 0.19 or even 0 under the left pointing. As it is well known, the manual parameter adjustment affects the noise filtering efficiency and accuracy; therefore, it was necessary to combine the PSO algorithm with the photon cloud noise filtering algorithm to determine the optimal parameters for the given test data.

Moreover, the noise filtering results of the two algorithms were better under laser center pointing than under laser left pointing. By analyzing the photon cloud data under different laser pointing, it is obviously discernible that the ground and canopy photons under center pointing. Hence, a higher density of signal photons improved the noise filtering ability of both algorithms.

In summary, both qualitative and quantitative results indicated that the PSODBSCAN algorithm performed better than the localized statistics algorithm in noise photon filtering under both center and left pointing.

4.3. Noise Removal Results of Different Algorithms

The mean statistical indicators of noise filtering algorithms are given in Table 16.

Table 16. The mean statistical indicators of noise filtering algorithms.

Statistical Indicators	*R*	*P*	*F*
Localized statistics algorithm	0.6802	0.8016	0.6978
PSODBSCAN algorithm	0.9994	0.9560	0.9759

The noise filtering experiments were conducted at different laser pointing and different beam types. The qualitative analysis results are shown in Figures 3–6. The visual analysis showed that the results of the PSODBSCAN algorithm contained fewer noise photon than that of the localized statistics algorithm. Thus, the PSODBSCAN algorithm described the coverage of canopy vegetation and the change in the ground more clearly, especially in the case of strong beam and center pointing (see Figure 3).

The quantitative analysis results are summarized in Table 16. In the noise filtering experiments, the PSODBSCAN algorithm achieved the mean *R*, *P*, and *F* values of 0.9994, 0.9560, and 0.9759, respectively, and the localized statistics algorithm achieved the mean *R*, *P*, and *F* values of 0.6802, 0.8016, and 0.6978, respectively. In fact, the localized statistics algorithm had a large variation range of *F* value (*F* was

0.99 under the center pointing and strong beam, and it was 0 under the left pointing and weak beam). Such results indicated that the localized statistics algorithm was greatly affected by the change in the photon density. Correspondingly, the localized statistics algorithm obtained high noise filtering accuracy under the high signal photon density, but it failed in the photon cloud noise filtering test at the low signal photon density. On the contrary, the PSODBSCAN algorithm consistently maintained a high noise filtering accuracy without manual parameters adjustment.

In general, both qualitative and quantitative evaluation results showed that the PSODBSCAN algorithm performed better in noise photon filtering than the localized statistics algorithm. This can be explained by the two following reasons. First, the PSODBSCAN algorithm clustered signal photons by using photon density rather than by using a certain threshold. Second, under different experimental conditions, by using manual adjustment of the noise filtering algorithm parameters it was difficult to obtain an optimal filtering effect. Therefore, the parameter adjustment was very critical in the noise filtering experiment. At the same time, it was proven that the PSODBSCAN algorithm achieved high noise filtering accuracy without manual parameters adjustment.

Ultimately, the result proved that the noise filtering effect of both algorithms depended on the photon density of the MATLAS data because the MATLAS technology is still in the airborne simulation stage. Based on the obtained results, the localized statistics algorithm can be useful for rapid noise photon filtering achieving a moderate accuracy, but this algorithm results in loss of signal photons at a low density of photon cloud. Thus, it can be used for rapid noise filtering at a high density of signal photons (e.g., strong beam and center pointing) but it requires a clear threshold for classification of noise and signal photons. Moreover, in the applications involving the MATLAS data, the PSODBSCAN algorithm represents a more convenient solution because it can largely retain the ground and canopy details achieving a much higher noise filtering accuracy at different laser pointing and beam types, which is extremely valuable in an automatic method. Accordingly, due to the proven usefulness for photon cloud processing of the proposed algorithm, it can be successfully implemented over the studied locations.

5. Conclusions

In this paper, the PSODBSCAN algorithm is proposed for accurate noise filtering in the forest region for simulated photon-counting Lidar data. The proposed noise filtering algorithm was validated by the experiments with the MATLAS data at different laser pointing and beam types on the same route over the forest region. Based on the results, the following conclusions can be drawn:

(1) At all laser intensities and laser pointing types, the PSODBSCAN algorithm performed better than the localized statistics algorithm.
(2) The PSODBSCAN algorithm did not need manual adjustment of parameters for different test data; thus, it had better applicability than the localized statistics algorithm.

These conclusions denote valuable information for noise filtering in forest regions using the photon-counting Lidar data. Nevertheless, there are still many issues to be addressed in the future. Since ATLAS is still in the research stage, there is no official accuracy-evaluation standard for noise filtering algorithms. It is expected that future research will propose a recognized accuracy-evaluation standard for noise filtering algorithms. The amount of ICESat-2 data covering the whole world would be huge, which represents the main challenge of photon noise filtering. Therefore, the development of a more effective and accurate noise removal algorithm will be the subject of our future work.

Author Contributions: J.H., Y.X. and L.Q. conceived and designed the experiments; J.H. performed the experiments; J.H. and Y.X. analyzed the data; L.Q. contributed materials; J.H., Y.X. and H.Y. wrote the paper. Y.X. and H.Y. secured funding for the project. J.T. and J.M. polished the language of the manuscript.

Funding: This work is supported by the National Key R&D Program of China (Granted: 2017YFD0600904), and the Key Laboratory of Satellite Mapping Technology and Application, National Administration of Surveying, Mapping and Geoinformation (KLSMTA-201706).

Acknowledgments: The authors would like to thank the ICESat-2 Project Science Office at NASA/GSFC for providing the MATLAS data used in this study. We also thank the editor and anonymous reviewers for reviewing our paper.

Conflicts of Interest: The authors declare no conflict of interest.

References

1. ICESat-2 Mission Brochure. Available online: https://icesat-2.gsfc.nasa.gov/sites/default/files/page_files/ICESat2missionBrochureFINAL1.pdf (accessed on 23 July 2018).
2. Amy, N.; Lori, A. The Potential Impact of Vertical Sampling Uncertainty on ICESat-2/ATLAS Terrain and Canopy Height Retrievals for Multiple Ecosystems. *Remote Sens.* **2016**, *12*, 1039. [CrossRef]
3. Jasinski, M.F.; Stoll, J.D.; Cook, W.B.; Ondrusek, M.; Stengel, E.; Brunt, K. Inland and Near-Shore Water Profiles Derived from the High-Altitude Multiple Altimeter Beam Experimental Lidar (MABEL). *J. Coast. Res.* **2016**, *76*, 44–55. [CrossRef]
4. Wang, X.; Pan, Z.; Glennie, C. A Novel Noise Filtering Model for Photon-Counting Laser Altimeter Data. *IEEE Geosci. Remote Sens. Lett.* **2016**, *13*, 947–951. [CrossRef]
5. Kelly, M.; Thomas, A.; Kaitlin, M.; Thorsten, M. Determination of Local Slope on the Greenland Ice Sheet Using a Multi beam Photon-Counting Lidar in Preparation for the ICESat-2 Mission. *IEEE Geosci. Remote Sens. Lett.* **2013**, *11*, 935–939. [CrossRef]
6. LI, G.; HUANG, J.; TANG, X.; Huang, G.; Zhou, S.; Zhao, Y. Influence of Range Gate Width on Detection Probability and Ranging Accuracy of Single Photon Laser Altimetry Satellite. *Acta Geod. Et Cartogr. Sin.* **2018**, *47*, 1487–1494. [CrossRef]
7. ICESAT-2: MABEL DOCUMENTATION. Available online: https://icesat-2.gsfc.nasa.gov/icesat2/legacy-data/mabel/docs/MABEL_Release_010_Note.pdf (accessed on 5 November 2014).
8. ICESAT-2: MATLAS DOCUMENTATION. Available online: https://icesat-2.gsfc.nasa.gov/icesat2/legacy-data/matlas/docs/Slides20141204.pdf (accessed on 4 December 2014).
9. David, H. Release 5 Data Product Documentation and Instrument Description [EB/OL]. Available online: https://icesat-2.gsfc.nasa.gov/icesat2/legacy-data/simpl/docs/SIMPL_2015_Rel5_Documentation_v1.1.pdf (accessed on 30 March 2016).
10. Dabney, P.; Harding, D.; Abshire, J.; Huss, T.; Jodor, G.; Machan, R.; Marzouk, J.; Rush, K.; Seas, A.; Shuman, C.; et al. The Slope Imaging Multi-polarization Photon-counting Lidar: Development and performance results. *Geosci. Remote Sens. Symp. IEEE* **2010**, 653–656. [CrossRef]
11. Magruder, L.; Neuenschwander, A. Noise filtering techniques for photon-counting ladar data. *Proc. Spie Int. Soc. Opt. Eng.* **2012**, *8379*, 1–9. [CrossRef]
12. Xia, S.; Wang, C.; Xi, X. Point cloud filtering and tree height estimation using airborne experiment data of ICESat-2. *J. Remote Sens.* **2014**, *18*, 1199–1207. [CrossRef]
13. Xu, Y. Research on Data Processing Technology of Single Photon Laser Altimetry. Master's Thesis, Xi'an University of Science and Technology, Xi'an, China, 2017.
14. Tang, H.; Swatantran, A.; Barrett, T.; DeCola, P.; Dubayah, R. Voxel-Based Spatial Filtering Method for Canopy Height Retrieval from Airborne Single-Photon Lidar. *Remote Sens.* **2016**, *8*, 771. [CrossRef]
15. Nie, S.; Wang, C.; Xi, X.; Luo, S.; Li, G.; Tian, J.; Wang, H. Estimating the vegetation canopy height using micro-pulse photon-counting LiDAR data. *Opt. Express* **2018**, *26*, 520–540. [CrossRef] [PubMed]
16. Herzfeld, U.C.; Trantow, T.M.; Harding, D.; Dabney, P.W. Surface-Height Determination of Crevassed Glaciers Mathematical Principles of an Autoadaptive Density-Dimension Algorithm and Validation Using ICESat-2 Simulator (SIMPL) Data. *IEEE Trans. Geosci. Remote Sens.* **2017**, *99*, 1–23. [CrossRef]
17. Herzfeld, U.C.; McDonald, B.W.; Wallin, B.F.; Neumann, T.A.; Markus, T.; Brenner, A.; Field, C. Algorithm for Detection of Ground and Canopy Cover in Micropulse Photon-Counting Lidar Altimeter Data in Preparation for the ICESat-2 Mission. *IEEE Trans. Geosci. Remote Sens.* **2014**, *52*, 2109–2125. [CrossRef]
18. Popescu, S.; Zhou, T.; Nelson, R. Photon counting LiDAR: An adaptive ground and canopy height retrieval algorithm for ICESat-2 data. *Remote Sens. Environ.* **2018**, *208*, 154–170. [CrossRef]
19. Zhang, J.; Kerekes, J. An Adaptive Density-Based Model for Extracting Surface Returns from Photon-Counting Laser Altimeter Data. *IEEE Geosci. Remote Sens. Lett.* **2014**, *12*, 726–730. [CrossRef]

20. Chen, B.; Pang, Y.; Li, Z.; Lu, H.; Liu, L.; North, P.; Rosette, J. Ground and Top of Canopy Extraction from Photon Counting LiDAR Data Using Local Outlier Factorwith Ellipse Searching Area. *IEEE Geosci. Remote Sens. Lett.* **2019**. [CrossRef]
21. De, B.; Develder, C.; Dhaene, T.; Deschrijver, D. Detection of unidentified appliances in non-intrusive load monitoring using siamese neural networks. *Int. J. Electr. Power Energy Syst.* **2019**, *104*, 645–653. [CrossRef]
22. Feng, S.; Xiao, W. Research and improvement of DBSCAN clustering algorithm. *J. China Univ. Min. Technol.* **2008**, *37*, 105–111.
23. Liu, S.; Meng, D.; Wang, X. DBSCAN algorithm based on grid cells. *J. Jilin Univ. Eng. Ed.* **2014**, *44*, 1135–1139. [CrossRef]
24. Li, X.; Yu, X.; Yang, C. Analysis of passenger aggregation characteristics of urban rail stations based on DBSCAN algorithm. *Control Decis.* **2019**, *34*, 18–24. [CrossRef]
25. Zhu, Y.; Luo, X.; Qu, K.; Tao, Y.; Lin, J.; Lin, H. Automatic recognition of tooth features based on DBSCAN and K-Means hybrid clustering. *J. Comput. Aided Des. Graph.* **2018**, *30*, 1276–1283. [CrossRef]
26. Peng, B.; Shi, C.; Gao, W. DBSCAN algorithm optimization and its application in village management decision. *J. Agric. Mach.* **2016**, *47*, 346–350. [CrossRef]
27. Wang, Y. Barrier-Constrained DBSCAN Algorithm Based on Particle Swarm Optimization. Master's Thesis, Harbin University of Engineering, Harbin, China, 2011.
28. Li, N.; Zhu, X.; Pan, Y.; Zhan, P. SVM remote sensing image classification optimized by artificial bee colony algorithm. *J. Remote Sens.* **2018**, *22*, 559–569. [CrossRef]
29. Tian, Z.; Ren, Y.; Wang, G. Short-term wind speed prediction based on improved PSO algorithm optimized EM-ELM. *Energy Sources* **2018**, 1–21. [CrossRef]
30. Ramarao, G.; Chandrasekaran, K. Evaluating Lightning Channel-Base-Current Function Parameters for Identifying Interdependence of Wavefront and Tail by PSO Method. *IEEE Trans. Electromagn. Compat.* **2018**, 1–8. [CrossRef]
31. Sui, X.; Wan, K.; Zhang, Y. Pattern Recognition of SEMG Based on Wavelet Packet Transform and Improved SVM. *Int. J. Light Electron Opt.* **2019**, *176*, 228–235. [CrossRef]
32. Wang, Y.Y.; Peng, W.X.; Qiu, C.H.; Jiang, J.; Xia, S.R. Fractional-order Darwinian PSO-Based Feature Selection for Media-Adventitia Border Detection in Intravascular Ultrasound Images. *Ultrasonics* **2018**. [CrossRef] [PubMed]
33. Shi, Y.; Eberhart, R. A modified particle swarm optimizer. In Proceedings of the IEEE International Conference on Evolutionary Computation, Anchorage, AK, USA, 4–9 May 1998; pp. 69–73. [CrossRef]
34. Shi, Y.; Eberhart, R.C. Parameter selection in particle swarm optimization. *Evol. Program.* **1998**, *3*, 591–600. [CrossRef]
35. Shi, Y.; Eberhart, R. Monitoring of particle swarm optimization. *Front. Comput. Sci. China* **2009**, *3*, 31–37. [CrossRef]
36. Deb, S.; Tian, Z.; Fong, S.; Wong, R.; Millham, R.; Wong, K.K. Elephant search algorithm applied to data clustering. *Soft Comput.* **2018**, *22*, 6035–6046. [CrossRef]
37. Ester, M.; Kriegel, H.; Xu, X. A density-based algorithm for discovering clusters a density-based algorithm for discovering clusters in large spatial databases with noise. *Int. Conf. Knowl. Discov. Data Min.* **1996**, *96*, 226–231.
38. Ferrara, R.; Virdis, S.G.; Ventura, A.; Ghisu, T.; Duce, P.; Pellizzaro, G. An automated approach for wood-leaf separation from terrestrial LIDAR point clouds using the densit based clustering algorithm DBSCAN. *Agric. For. Meteorol.* **2018**, *262*, 434–444. [CrossRef]
39. Chen, Y.; Tang, S.; Bouguila, N.; Wang, C.; Du, J.; Li, H. A Fast Clustering Algorithm based on pruning unnecessary distance computations in DBSCAN for High-Dimensional Data. *Pattern Recognit.* **2018**, *83*, 375–387. [CrossRef]
40. Ruske, S.; Topping, D.O.; Foot, V.E.; Morse, A.P.; Gallagher, M.W. Machine learning for improved data analysis of biological aerosol using the WIBS. *Atmos. Meas. Tech.* **2018**, *11*, 6203–6230. [CrossRef]